Cone Photoreceptors Develop Normally in the Absence of Functional Rod Photoreceptors in a Transgenic Swine Model of Retinitis Pigmentosa

Juan P. Fernandez de Castro,[1] Patrick A. Scott,[1,2] James W. Fransen,[2] James Demas,[3] Paul J. DeMarco,[4] Henry J. Kaplan,[1] and Maureen A. McCall[1,2]

[1]Department of Ophthalmology and Visual Sciences, University of Louisville, Louisville, Kentucky, United States
[2]Department of Anatomical Sciences and Neurobiology, University of Louisville, Louisville, Kentucky, United States
[3]Department of Biology, St. Olaf College, Northfield, Minnesota, United States
[4]Department of Psychological and Brain Sciences, University of Louisville, Louisville, Kentucky, United States

Correspondence: Maureen A. McCall, Department of Ophthalmology and Visual Sciences, University of Louisville School of Medicine, 301 E. Muhammad Ali Boulevard, Louisville, KY 40204, USA; mo.mccall@louisville.edu.

JPFdC and PAS contributed equally to the work presented here and should therefore be regarded as equivalent authors.

Submitted: December 6, 2013
Accepted: February 27, 2014

Citation: Fernandez de Castro JP, Scott PA, Fransen JW, et al. Cone photoreceptors develop normally in the absence of functional rod photoreceptors in a transgenic swine model of retinitis pigmentosa. *Invest Ophthalmol Vis Sci*. 2014;55:2460–2468. DOI:10.1167/iovs.13-13724

Purpose. Human and swine retinas have morphological and functional similarities. In the absence of primate models, the swine is an attractive model to study retinal function and disease, with its cone-rich visual streak, our ability to manipulate their genome, and the differences in susceptibility of rod and cone photoreceptors to disease. We characterized the normal development of cone function and its subsequent decline in a P23H rhodopsin transgenic (TgP23H) miniswine model of autosomal dominant RP.

Methods. Semen from TgP23H miniswine 53-1 inseminated domestic swine and produced TgP23H and Wt hybrid littermates. Retinal function was evaluated using ERGs between postnatal days (P) 14 and 120. Retinal ganglion cell (RGC) responses were recorded to full-field stimuli at several intensities. Retinal morphology was assessed using light and electron microscopy.

Results. Scotopic retinal function matures in Wt pigs up to P60, but never develops in TgP23H pigs. Wt and TgP23H photopic vision matures similarly up to P30 and diverges at P60 where TgP23H cone vision declines. There are fewer TgP23H RGCs with visually evoked responses at all ages and their response to light is compromised. Photoreceptor morphological changes mirror these functional changes.

Conclusions. Lack of early scotopic function in TgP23H swine suggests it as a model of an aggressive form of RP. In this mammalian model of RP, normal cone function develops independent of rod function. Therefore, its retina represents a system in which therapies to rescue cones can be developed to prolong photopic visual function in RP patients.

Keywords: retina, retinitis pigmentosa, swine, electrophysiology, electron microscopy

Species can be divided into altricial (helpless) and precocial (freely moving) based on their abilities at birth. Altricial animals, like cats,[1,2] dogs,[3,4] rats,[5–10] rabbits,[11,12] and mice,[13] are born with closed eyelids that open at approximately 2 weeks of age.[14] Their retinas mature after birth, developing the normal laminar structure and complement of cell classes.[3,9] Near the end of this maturation process, opsins are expressed by the photoreceptors. Retinal function arises at approximately the time of eye-opening and matures over the next 2 to 3 weeks,[14] as evident with ERG measures.

In contrast, precocial animals, like primates, humans,[15] and pigs, are born with mature retinal cell classes and lamination patterns,[16,17] although changes related to foveal development occur postnatally. In humans, both ERG function[18] and visual perception develop postnatally.[19] The domestic pig (*Sus scrofa domesticus*) and human retina share other similarities.[15,20–26] The swine has a cone-rich visual streak and humans have a highly specialized fovea.[27–29] In both, these areas correspond to an area with a high density of retinal ganglion cells (RGCs).[29] Swine and humans share a similar spatial distribution of their rod photoreceptors,[25,26] and their medium- and short-wavelength cone photoreceptors, although humans also have a third cone photoreceptor not found in swine.

To date, our understanding about changes that occur in most retinal diseases comes from work in altricial species, in particular in rodents, because they represent inbred lines, their genome has been easily manipulated, and they have rapid generation time and large litters. These results have been crucial to our understanding of disease progression and mechanism. However, altricial species do not recapitulate human development and aging, and the rodent retina does not contain a cone-rich region. Several similarities in eye and retinal physiology and anatomy, as well as the relatively new ability to manipulate the swine genome, make the pig an increasingly attractive translational model for human retinal disease.[30] For example, they are now used to test retinal implants[31] and transplants,[32] and study retinal capillary disease in diabetic retinopathy,[33] ischemia reperfusion,[23] and material biocompatibility.[24]

To create a large animal RP model in which to apply these approaches, we developed and characterized transgenic (Tg) miniature swine with a proline-to-histidine substitution at amino acid residue 23 in rhodopsin (P23H).[34] One of the severely affected TgP23H founders, 53-1, had virtually no rod-driven

function at the earliest age tested, 3 months,[34] and cone-driven function that slowly declined and had residual function at approximately 2 years of age. In a companion study,[35] we show that rod photoreceptor morphology is compromised in TgP23H embryos and rod function is absent at postnatal day (P)3. In this study, we also characterized similar F1 hybrid offspring, resulting from a cross of 53-1 to domestic swine. We show that rod function never develops and that despite the absence of rod function, cone function develops similar to Wt up to P30 and then begins a slow decline. Although this is not the common progression of human autosomal dominant P23H RP, changes in early postnatal retinal function occur in some autosomal recessive cases of RP.[36–38] Our results suggest that this transgenic model of aggressive RP always lacks rod function, but cone function develops similar to Wt and its decline is slow and emulates the decline in many forms of RP. Thus, it may be useful in the development of therapeutic strategies for the preservation of cone function in those diseases.

Materials and Methods

Animals

To create large litter sizes with sufficient matched Wt and Tg littermates to study at several time points, Wt domestic (Do) sows were artificially inseminated with sperm from TgP23H 53-1[34] National Institutes of Health (NIH) cc inbred haplotype to create F1 hybrid (DoXcc) swine. A blood sample was taken and DNA isolated at P1 from all offspring and they were genotyped via PCR using reaction conditions and rhodopsin primers described previously.[34] All experimental protocols were approved by the University of Louisville Institutional Animal Care and Use Committee and adhere to the ARVO Statement for Use of Animals in Ophthalmic and Vision Research. Table 1 shows the numbers of Wt and TgP23H pigs used in experiments at each age.

Preparation for ERG Recordings

Preparation for full-field (ff) and multifocal (mf) ERGs in pigs older than P30 have been described previously.[34] Briefly, they were sedated and anesthetized via intravenous (IV) administration of a mixture of ketamine (5 mg/kg), dexmedetomidine (0.02 mg/kg), and atropine (0.025 mg/kg). In piglets younger than P30, isoflurane was administered via a mask placed over the nose and mouth to induce anesthesia. In all pigs, once a stable plane of anesthesia was reached, an IV catheter was placed in the ear vein and used to deliver IV fluids (Lactated Ringers Solution with or without 5% dextrose; 10–15 mL/kg/h), to maintain blood pressure and normal glycemic levels (60–140 mg/dL). Anesthesia was maintained with 1% to 3% isofluorane[39] administered via endotracheal tube for animals older than 14 days and a tight mask for younger piglets. Vital signs (oxygen saturation, respiratory rate, heart rate, and blood pressure) and body temperature were monitored and maintained within the normal range throughout the experiment. Pupils were dilated and accommodation relaxed with topical applications of 2.5% phenylephrine hydrochloride and 1% Tropicamide drops. Adjustable lid speculae were used to keep the eyelids separated.

Full-Field Flash ERG

The procedure for recording and analyzing ffERGs has been previously published.[34] Flashes were produced and responses recorded using a UTAS ERG system with a BigShot Ganzfeld (LKC Technologies, Inc., Gaithersburg, MD, USA) stimulator. The swine's head was placed inside of the ganzfeld bowl and bilateral ERGs recorded using ERG-Jet electrodes (LKC Technologies, Inc.) placed on the cornea. The cornea was kept moist by covering it with hypromellose solution 2.5%. A ground electrode was placed behind the ear and a reference electrode on the midline of the forehead. The stimulus protocol was based on the International Society for Clinical Electrophysiology of Vision standard for clinical ffERG.[40] Briefly, after 20 minutes of dark-adaptation, the ffERG was recorded to strobe flash intensities of 0.01 cd·s·m^{-2} with an interstimulus interval (ISI) of 2 seconds (15 samples) to isolate the rod scotopic response. The animal was light adapted for 10 minutes to a 20 cd·m^{-2} background and the standard photopic cone ERG response recorded at 3 cd·s·m^{-2} and 0.5 seconds ISI (30 samples). Cone responses were also measured to a 3 cd·s·m^{-2} 30-Hz flicker stimulus (30 samples). Individual responses were analyzed and aberrant waveforms rejected before averaging. From the average response, the a-wave was measured from baseline to trough and b-wave from trough to peak. The latency was measured from stimulus onset to a-wave trough or b-wave peak.

Table 1. Number of Animals of Each Genotype at Each Time Point

	ffERG–mfERG		MEA	
Age, d	P23H	Wt	P23H	Wt
3	4	5	1	2
14	3	6	2	2
30	6	11	2	4
60	7	8	4	3
90	6	5	2	3
120	6	4	0	0

Multifocal ERG

The procedure for recording and analyzing mfERGs has been previously published.[34] A FMS III VERIS System (Electrodiagnostic, Inc., Redwood City, CA, USA) was used to record mfERGs in animals of P60 or older. A DTL electrode (Diagnosys, Lowell, MA, USA) was looped around the cornea and covered with a rigid gas-permeable contact lens for the recording. Moisture was maintained with artificial tears (Tears Again; OCuSOFT, Inc., Rosenberg, TX, USA). Reference and ground electrode placement have been described above for ffERGs. To minimize eye movements, a stay suture was placed in the conjunctiva and a retrobulbar block was performed to minimize eye movement during the recording. An unscaled stimulus pattern was centered on the visual streak, 3.6° above the superior edge of the optic disc, which was located in the lower corner (right or left depending on the eye). To ensure that the stimulus position was maintained throughout the recording, an image of the fundus was taken and the position of the optic disc and vessels overlaid on the fundus image and adjusted for any drift. The stimulus covered the entire horizontal extent of the visual streak and consisted of 103 hexagonal elements that flickered on and off and were presented for 7 minutes. The spatial density profile for the photoreceptor response was obtained, as were topographic and response amplitude maps, which were calculated by averaging the individual N1-P1 amplitudes as described previously.[34] Responses in both nasal and temporal retina were recorded and averaged to obtain a single value per eye.

Multielectrode Array Recordings of Spontaneous and Visually Evoked Responses of RGCs

Piglets were anesthetized (described above), killed with a solution of Beuthanasia (1 mL/5 kg), and their eyes were enucleated. The left eye from each animal was processed for standard histology and transmission electron microscopy. The

Investigative Ophthalmology & Visual Science

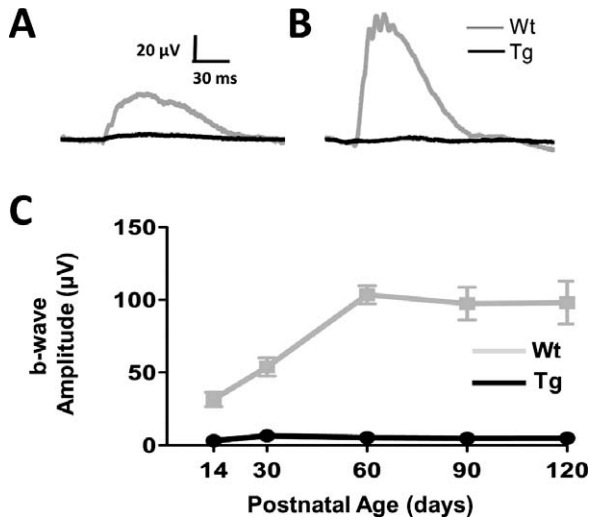

Figure 1. Rod-driven ff-ERG responses never develop in TgP23H swine. (**A**, **B**) Representative ERG responses to a scotopic flash in dark-adapted Wt and TgP23H swine at P14 (*left*) and at P90 (*right*). (**C**) Mean b-wave responses as a function of age show that a rod-driven response never develops in TgP23H swine and that Wt scotopic responses reach maturity at P60.

eyecup of the right eye was dissected and the anterior chamber and vitreous removed in oxygenated Ames medium (Sigma-Aldrich, St. Louis, MO, USA) at 4°C. Eyecups were placed in a light tight container (~10 minutes) and the retina was dissected from the pigment epithelium, under dim red light. A piece of the retina (3 × 3 mm) was removed and transferred onto a 200/30iR-Ti-gr 60 electrode multielectrode array (Multi Channel Systems, Reutlingen, Germany), RGC side down. The chamber containing the retina on the array was continuously superfused with oxygenated Ames held at 32°C with a PH01 heated perfusion cannula and integrated heating system (Multi Channel Systems).

The retina was held in the recording chamber for 1 hour before recording. Spontaneous spiking activity was recorded in the dark for 30 minutes or more. Full-field, achromatic light flashes (2-second duration/10 presentations/ISI 60s) were presented to evoke a rod-driven response (0.015 µW/cm^2). Cone-driven responses were assessed with both 0.15 and 1.5 µW/cm^2 flashes (2-second duration/10 presentations/ISI 60s). RGC spike trains were recorded, stored, and sorted offline. Spikes with amplitudes 6 SDs above baseline noise were isolated for each channel using MC Rack (Multi Channel Systems) and then transferred to Offline Sorter (Plexon, Dallas, Texas, USA), where they were grouped into individual cells, using principal components analysis. Data were imported into Neuroexplorer (Nex Technologies, Madison, AL, USA). Responses to full-field light stimuli were averaged and binned and poststimulus time histograms (PSTHs) created along with raster plots to show responses to individual stimulus presentation. The averaged PSTHs were used to quantify the peak firing rate for each cell.

Tissue Preparation for Morphological Analyses

Piglets were euthanized (described above) at the end of an ERG evaluation, their eyes were enucleated and immersion fixed in 2% paraformaldehyde/2% glutaraldehyde in phosphate (PO_4) buffer (0.1 M, pH 7.4) for 24 hours at 4°C.

Retinal tissue was dissected and processed as previously described.[35,41] Briefly, a 3-mm-wide strip of retinal tissue was dissected along the vertical and horizontal meridian to include the optic disc and ora serrata. Retinal tissue was dehydrated in a series of ascending ethanol concentrations and stored overnight at 4°C in JB-4 infiltrating solution (Ted Pella, Redding, CA, USA) and then embedded in blocks of JB-4 Plus resin (Ted Pella). Blocks of retinal tissue were cut into 4-µm semithin sections using a Leica EMUC6 Ultramicrotome (Leica Microsystems, Buffalo Grove, IL, USA), stained with 1% cresyl violet (Sigma-Aldrich), covered with a coverslip, and examined at ×40 or ×100 using a NIKON EFD-3 Episcopic-Fluorescence microscope (Nikon, Inc., Melville, NY, USA). A Moticam 2500 high-resolution digital camera (Motic, Richmond, British Columbia, Canada) was used to take photomicrographs and brightness and contrast were adjusted using Adobe Photoshop (Adobe Systems, San Jose, CA, USA).

Table 2. Implicit Times TgP23H and Wt a- and b-Waves

	Rod b-Wave, ms	Cone b-Wave, ms	
Age, d	Wt	Wt	Tg
3	76	24	22
14	76	24	23
30	74	24	23
60	68	23	23
90	53	21	23
120	51	20	22

Nuclear Cell Counts

Nuclear profile counts were performed to quantify photoreceptor loss in the outer nuclear layer (ONL) using a previously described technique.[41,42] Ten adjacent counts of vertical columns of photoreceptor nuclei in the ONL were made at 2-mm increments along the vertical and horizontal meridian, extending from the margin of the optic disc to the ora serrata, in at least five sections per location without knowledge of the genotype. The mean number of photoreceptor nuclei per vertical column in the ONL was calculated for each location. The overall mean number photoreceptor nuclei per vertical column in the ONL were calculated by averaging the mean number of photoreceptor nuclei per vertical column in the ONL across all locations in each eye and for each age.

Transmission Electron Microscopy

Preparation and processing of retinal tissue for examination by transmission electron microscopy has been described previously described.[35,41] Briefly, a 2 × 2-mm piece of tissue was dissected 5 mm above the superior margin of the optic disc. Retinal tissue was rinsed in buffer, postfixed in 2% osmium tetroxide and 1.5% potassium ferrocyanide in dH_2O for 2 hours, dehydrated in an ascending series of ethanols, and embedded in Epon-Araldite (Electron Microscopy Sciences, Hatfield, PA, USA). A diamond knife (Micro Star Technologies, Inc., Huntsville, TX, USA) was used to cut ultrathin sections (90 nm) on an ultramicrotome (Ultracut E 701704; Reichert-Jung, Buffalo, NY, USA). Ultrathin sections of retinal tissue were collected on copper grids and counterstained with 4% methanolic uranyl acetate (Electron Microscopy Sciences). Photoreceptor morphology was examined by electron microscopy using a transmission electron microscope (Model 300; Phillips, Eindhoven, The Netherlands). Photomicrographs were taken with a digital camera (15-megapixel digital camera; Scientific Instruments and Applications, Duluth, GA, USA) and the images processed with Maxim DL Version 5 software (Diffraction Limited, Ottawa, Ontario, Canada).

Investigative Ophthalmology & Visual Science

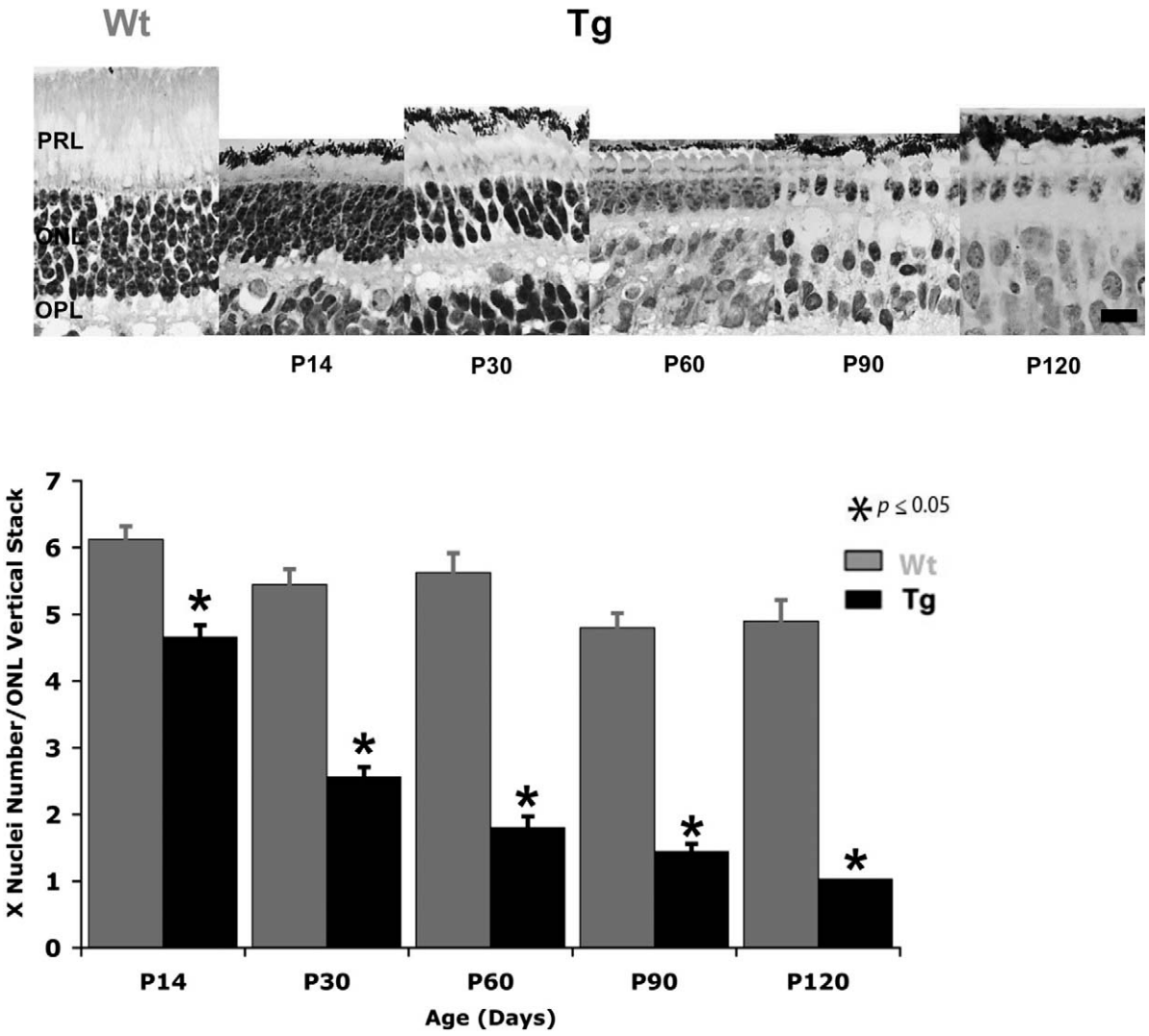

Figure 2. Rod photoreceptors degenerate within the first 3 months in TgP23H pigs. (**A**) Representative cresyl violet–stained sections of Wt at P120 and TgP23H retina from P14 to P120. There is a clear and rapid decline in the numbers of photoreceptor nuclei in the ONL, particularly between P14 and P30. (**B**) The histogram shows significant loss in the mean number of photoreceptor nuclei per vertical stack in the ONL of TgP23H retina at all ages compared with Wt. *Scale bar*: 10 μm. P14, $P < 0.001$; P30–P120, $P < 0.0001$.

Statistical Analyses

Statistical analyses of the ERG data was performed using Prism 5 (GraphPad Software, Inc., La Jolla, CA, USA). Unpaired *t*-tests were used to compare amplitudes of the waveforms and a *P* value less than or equal to 0.05 was interpreted as being statistically significant from age-matched Wt littermates. For multielectrode array (MEA) data, qualitative measures were calculated in Neuroexplorer (Nex Technologies) and exported to Prism 5 (GraphPad Software, Inc.) for statistical analysis. Data were analyzed using parametric statistics unless otherwise noted. Results were considered significant for a *P* value of less than or equal to 0.05. For retinal morphometric analyses, we used InStat 3 for Macintosh (GraphPad Software, Inc.).

Counts of the number of photoreceptor nuclei per vertical column in the ONL in Wt versus TgP23H were compared using unpaired *t*-tests with a *P* value of less than or equal to 0.05 considered a significant difference. Overall mean number of photoreceptor nuclei per vertical column in the ONL was compared across all ages using one-way ANOVA and post hoc *t*-tests.

Results

Rod Photoreceptor Function Never Develops as a Result of Early Changes in Rod Photoreceptor Number in TgP23H Swine

Wt hybrid swine have scotopic and photopic b-wave responses at P3.[35] TgP23H littermates had similar photopic responses at this age, but they lacked a scotopic b-wave.[35] To discriminate between a delay and a lack of development of a TgP23H hybrid scotopic response, we examined and compared scotopic ffERG responses from age-matched Wt and TgP23H hybrids between P14 and P120. Figures 1A through 1C show that a rod-driven ERG response never develops in the TgP23H retina. In contrast, Wt rod-driven ERG responses mature postnatally and adult b-wave response amplitudes are reached between P30 and P60. Along with the maturation in response amplitude, the scotopic b-wave implicit time also shortens, reaching mature levels at the same stage between P30 and P90 (Table 2).

We examined the same TgP23H retinas and found that morphological changes in the outer retina are consistent with

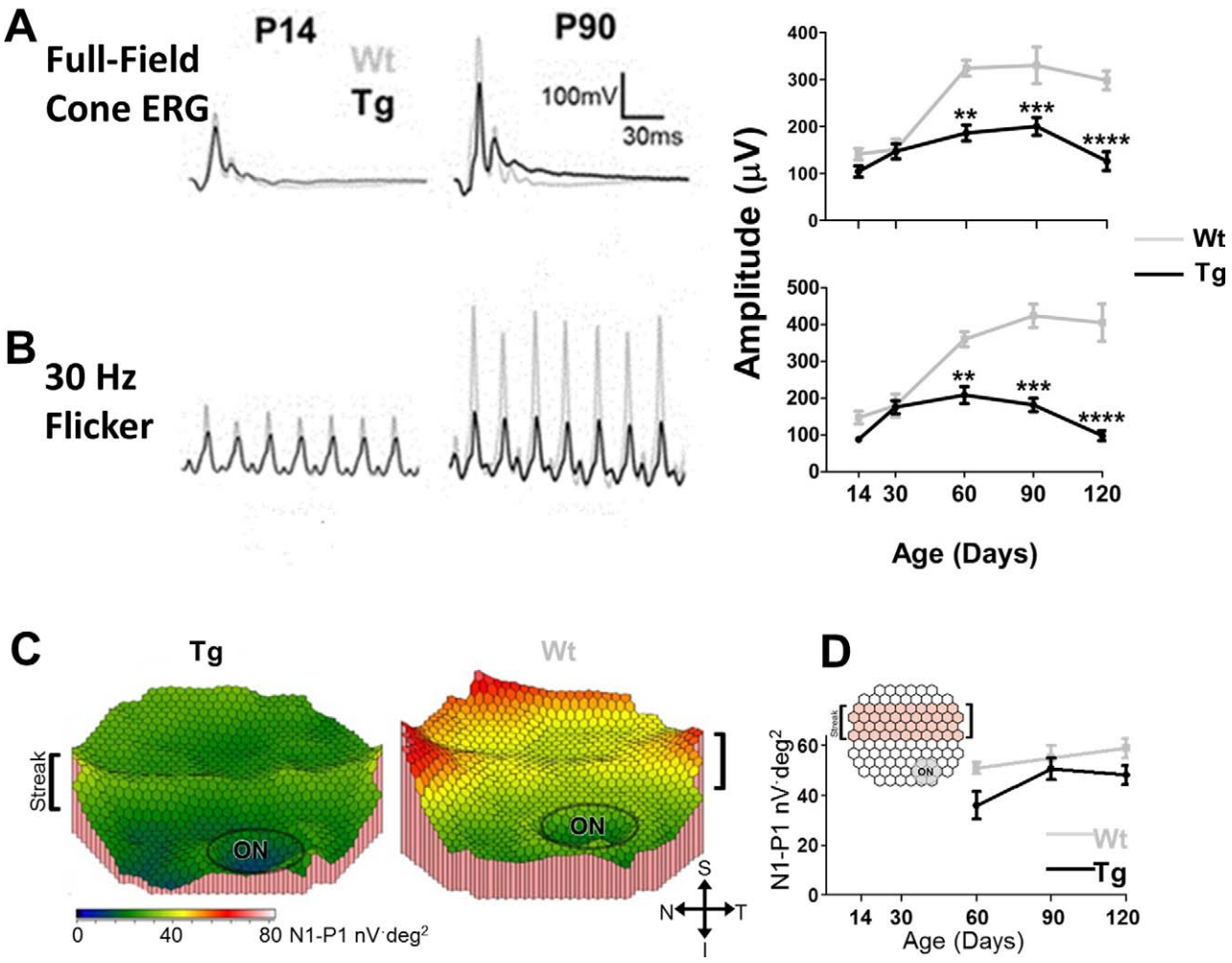

Figure 3. Cone-driven ERG responses in Wt and TgP23H mature normally up to P30 and then TgP23H responses decline. (**A**) Representative ERG responses at P14 and P90 to a photopic full-field flash (3 cd·s·m^{-2}). *Right graph* shows full-field cone ERG amplitude as a function of age. (**B**) Representative ERG responses to a full-field flicker (3 cd·s·m^{-2}) stimulus. (Note the baselines in the representative traces have been zeroed to overlay the data.) *Right graph* shows 30-Hz flicker ERG amplitude as a function of age. For both full-field and 30-Hz flicker ERGs, P14 TgP23H and Wt responses are similar. In Wt, the responses continue to mature until approximately P60. TgP23H response amplitudes plateau and then decline between P90 and P120. At P90, the ERG responses have similar waveforms, but TgP23H response amplitudes are reduced compared with Wt. (**C**) Representative topographic color maps showing TgP23H and Wt mfERG responses around the visual streak at P120 (optic nerve head [ON] is *circled* in the *lower right corner*). (**D**) Averaged mfERG amplitudes in TgP23H are significantly smaller than Wt at P120.

this functional defect. Figure 2 shows the significant decline in the number of photoreceptor nuclei from P14 to P120 (*t*-test, P14 $P < 0.001$; P30–P120 $P < 0.0001$). Based on their morphological characteristics, only a single layer of cone nuclei remained in the ONL at P90. The absence of a rod-driven ffERG between P14 and P120, along with the rapid degeneration of rod photoreceptors and our previous observations that a rod-driven response was absent at P3, indicates that a scotopic response failed to develop in the TgP23H swine.

Cone Photoreceptor Driven Function Develops Normally Despite the Absence of Rod Photoreceptor Function

In contrast to rod function at P3, we show that cone-driven ERG b-wave responses are similar between Wt and TgP23H hybrid littermates.[35] To define the normal development and decline of this photopic response, we examined and compared photopic ff- and mf-ERG responses of Wt and TgP23H hybrid swine at ages up to P120. Figures 3A and B show that cone driven flash and flicker ffERG responses from Wt and TgP23H littermates were similar up to P30. Thereafter, the Wt response continued to mature, reaching adult response amplitudes between P60 and P90. In contrast, the TgP23H photopic response amplitude plateaus between P30 and P90 and then declines. Both the TgP23H full-field b-wave and flicker response amplitudes are significantly smaller than Wt between P60, P90, and P120 (*t*-test; $P = 0.0025$, $P = 0.0018$, $P < 0.0001$, respectively).

We recorded mfERGs at age P60 and older. Figure 3C shows representative color response density maps of P60 Wt and TgP23H retinas in and around the visual streak, which is located superior to the optic nerve head (ON). In Wt animals, the n1-p1 mfERG response amplitude (Fig. 3D; averaged over the visual streak [see inset]) were relatively stable between P60 and 120, There was a trend in the TgP23H n1-p1 response amplitude to be smaller than Wt, but they differed significantly only at P120 (*t*-test, $P = 0.0199$).

We examined the ultrastructural morphology of cone photoreceptors to determine if functional and structural

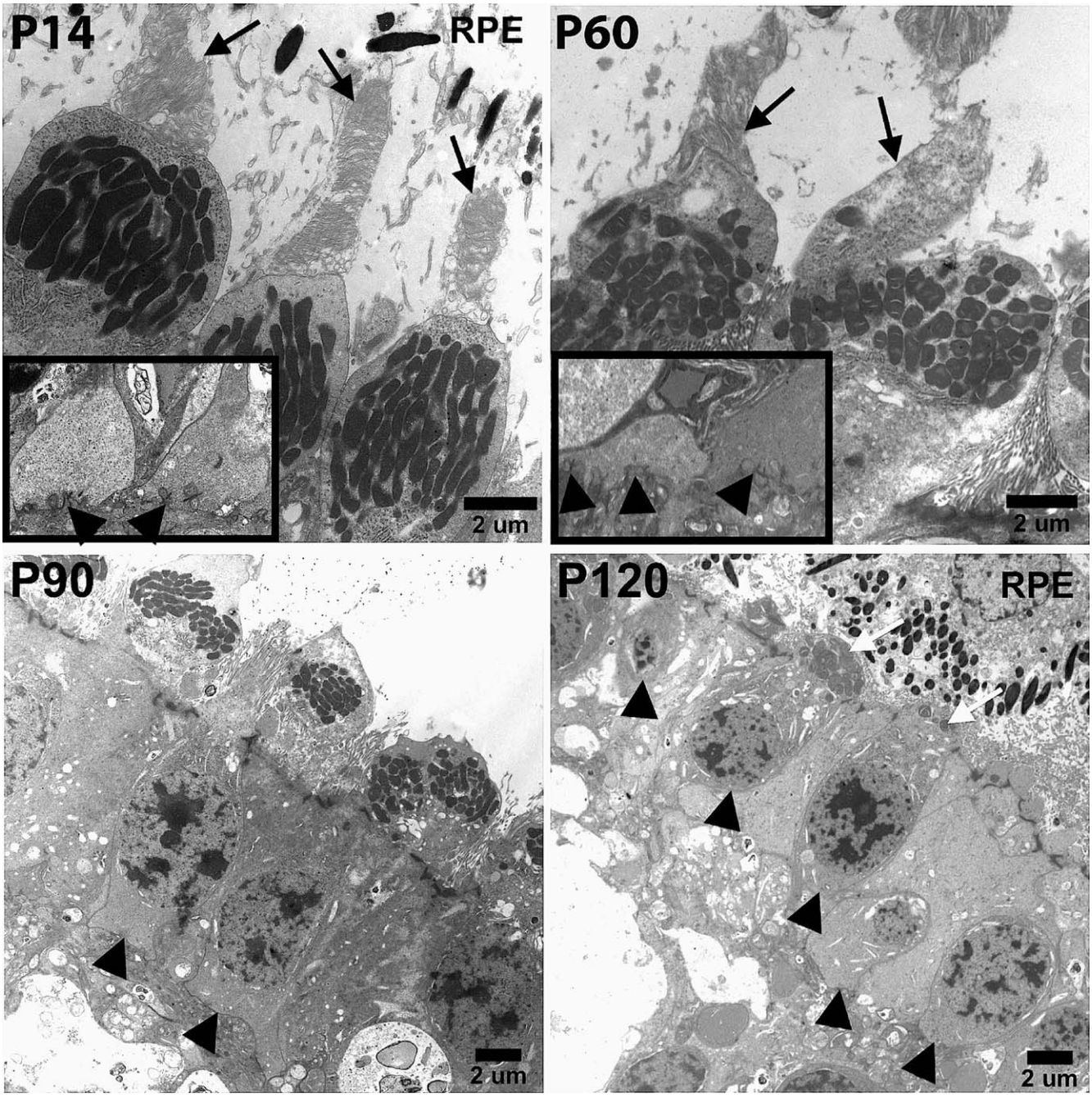

FIGURE 4. Abnormalities in TgP23H cone photoreceptor morphology arise at P60. Cone inner and outer segments (*black arrows*) and cone pedicles (inset: *black arrowheads*) are normal at P14. At P60 cone outer segments (*black arrows*) show irregular disc stacking and some loss of outer segment length, whereas triadic profiles appear normal (inset: *black arrowheads*). By P90, TgP23H cone photoreceptors lack outer segments, and triadic profiles in their pedicles are no longer apparent (*black arrowheads*). At P120, some TgP23H cones with inner segments remain (*white arrows*), but do not have pedicles (*black arrowheads*).

changes could be correlated (Fig. 4). We found that cone photoreceptor outer segment morphology appeared normal until P60. At P60, TgP23H cone outer segments began to show irregular disc stacking and the onset of outer segment degeneration. By P90, all cone photoreceptors lacked outer segments, although many retained inner segments. By P120, only a few cones retained inner segments but none had identifiable pedicles. Up to P60, TgP23H cones retained triadic profiles and synaptic ribbons. At and after P90 these were absent. The initial decline in retinal function was mirrored by changes in photoreceptor morphology. Although significant morphological changes were found at P120, the retina preserved a relatively robust photopic ERG.

Cone- but Not Rod-Driven Function Is Evident in RGC Visually Evoked Responses

To more selectively evaluate the impact of changes in outer retinal function on the retinal output, we recorded spontaneous and visually evoked responses of Wt and TgP23H RGCs by

Investigative Ophthalmology & Visual Science

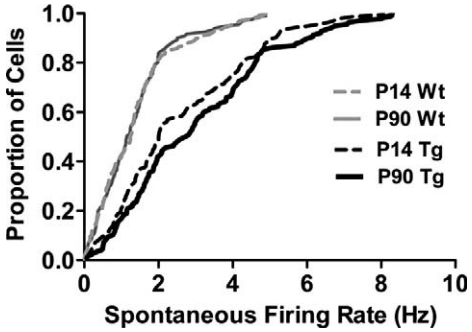

FIGURE 5. Spontaneous activity among TgP23H RGCs is significantly higher at all ages. Cumulative frequency curves of the spontaneous firing rates of Wt and TgP23H RGCs at the earliest time point (P14) and at P90. Responses were recorded under dark-adapted conditions and before any visual stimulation of the retina on the MEA. At these and all other ages, the TgP23H RGCs had significantly higher spontaneous rates (Kolmogorov-Smirnov, P14, KS = 0.1570, $P < 0.0001$; P90, KS = 0.1213, $P < 0.001$).

using an MEA. Similar to RGCs in rodent models of RP,[43] cumulative frequency curves (Fig. 5) show that spontaneous activity levels in TgP23H RGCs were significantly higher than Wt between P14 and P90 (Kolmogorov-Smirnov at every older time point, $P < 0.001$). This difference resulted from a much larger fraction of TgP23H RGCs with spontaneous firing rates above 2 Hz when compared with Wt.

Of the total number of RGCs with spontaneous activity, we determined the percentage of RGCs that also were visually responsive, using a bright full-field photopic stimulus (1.5 μW/cm^2). At every age, the percentage of visually responsive TgP23H RGCs was 50% or less of Wt (Fig. 6A). Using full-field stimuli at two lower intensities, we also observed changes in the sensitivity between Wt and TgP23H RGCs. Representative average PSTHs (Fig. 6Bi) from a Wt and a TgP23H RGC at P60 to a dim (rod-driven) stimulus (0.015 μW/cm^2) illustrate that Wt but not TgP23H RGCs are responsive. This is consistent with the lack of rod-driven responses as seen in the TgP23H ff-ERG. This result is quantified in the histograms to the right (Fig. 6Bii). All Wt RGCs responded to the intermediate intensity stimulus (0.15 μW/cm^2), whereas significantly fewer TgP23H RGCs responded. The remaining TgP23H RGCs responded to the brightest stimulus (1.5 μW/cm^2), although this was a much smaller percentage of the total RGCs (Fig. 6A).

As a final measure of the sensitivity of Wt and TgP23H RGCs, we compared their response peak amplitude to the 0.15 μW/cm^2 full-field stimulus (peak amplitude was corrected for spontaneous firing rates). We chose the intermediate stimulus intensity to reduce the possibility of response saturation in Wt RGCs to the brightest stimulus.

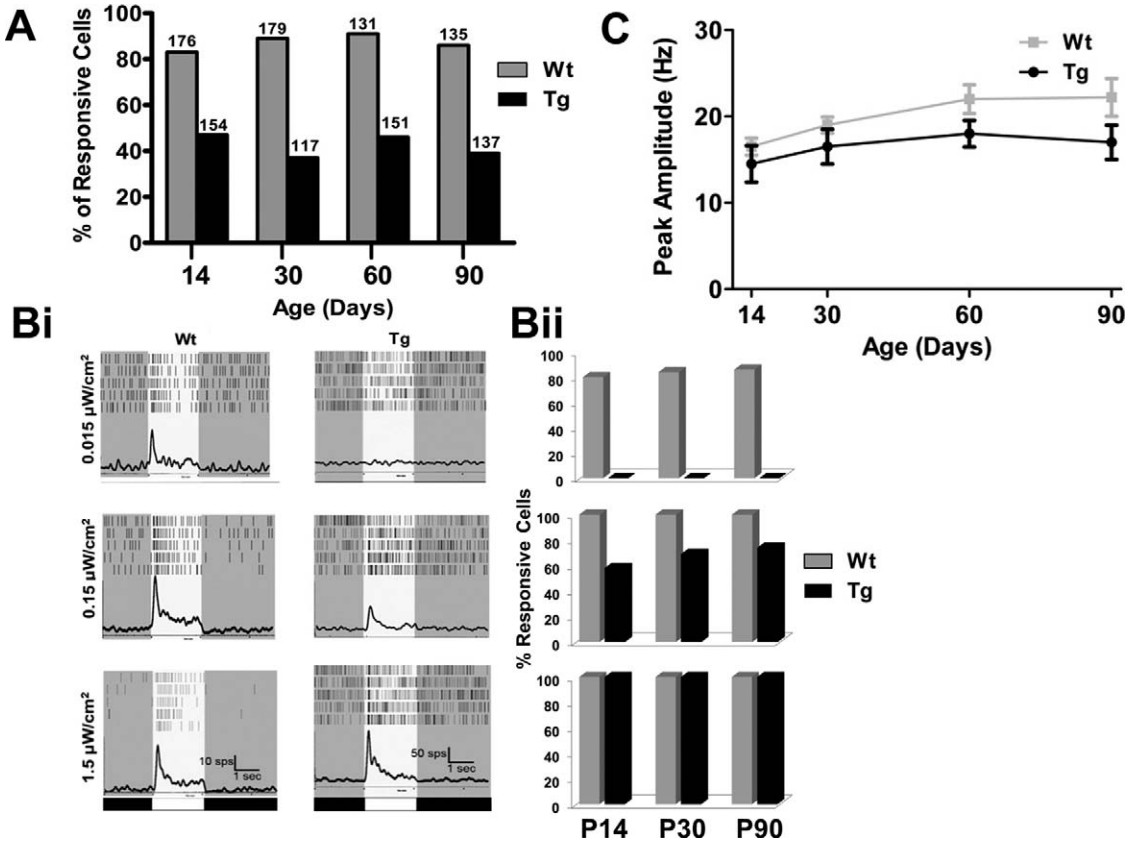

FIGURE 6. The percentage of visually responsive TgP23H RGCs and the light sensitivity of visually responsive Tg RGCs are lower than Wt. (**A**) Percentage of spontaneously active RGCs that also showed light-evoked responses. Numbers above columns are the total number of cells recorded at each age and genotype. Across age, the percentage of Wt RGCs with both spontaneous and visually evoked activity is significantly higher than in TgP23H RGCs. (**Bi**) Representative average Wt and TgP23H RGC PSTHs to increasing full-field stimulus intensity (0.015, 0.15, and 1.5 μW/cm^2). Note the *scale bar* changes between Wt and TgP23H PSTHs. Although the peak amplitude of the response appears larger in Tg swine, this was due to the higher spontaneous activity (see Fig. 5). (**Bii**) Histograms quantify the percentage of Wt and TgP23H RGCs that are responsive to each stimulus intensity. TgP23H RGCs do not respond to the dimmest stimulus, consistent with a lack of rod-driven activity. (**C**) The average peak amplitude of Wt and TgP23H RGCs to the middle-intensity stimulus (0.15 μW/cm^2) increase similarly with age up to P60. There appears to be a decline in TgP23H RGC responses at P90, but this did not differ significantly from Wt.

Once spontaneous activity levels were subtracted from the response, Wt and TgP23H RGCs had similar peak response across most time points (Fig. 6C). Consistent with the ERG responses, TgP23H RGC peak amplitudes began to decline at P90 but were still not statistically lower than Wt (P90 $P = 0.09$). Although many TgP23H RGCs become nonresponsive or lose light sensitivity even as early as P14, the visually responsive RGCs that remained had relatively robust responses to photopic stimulation. This represents a conundrum, because the cones that drove this response are grossly abnormal at later ages (>P60).

Discussion

Converging evidence from our measures of retinal function indicate that Wt swine retinal function develops after birth and reaches maturity between P60 and P90. In the Wt swine retina, rod and cone function develop in parallel, although a final maturation step in their cone function, related to the flicker response, may mature later. Humans also exhibit postnatal maturation of retinal function. Infants have smaller ERG amplitudes and longer implicit times than adults, with their a- and b-wave responses maturing systematically with age.[44,45] This is true for scotopic[46–48] and photopic[49] responses. The similarities in the development of the function of the Wt swine retina with humans strengthen the swine as a model system in which to study the development of cone responses.

In TgP23H swine, rod photoreceptor dysfunction is present as early as P3.[35] Despite the absence of rod pathway function and significant rod photoreceptor degeneration, the photopic ERG b-wave is normal, indicating that cone photoreceptor and bipolar cell function develop normally up to P30. Although not evident in the ERG results, we found that many TgP23H RGCs were visually nonresponsive as early as P14. This suggests that many cone-mediated RGC responses require an intact rod pathway to develop. Alternatively, there may be RGCs that are extremely insensitive and could not be driven by our brightest available stimulus (1.5 $\mu W/cm^2$).

Some of the hallmarks of RP in the TgP23H pig are similar to the more aggressive rodent models of RP, including the *rd1* mouse[50] and some lines of the P23H[51] and S334ter rat.[52] For example, both show morphological changes in rod photoreceptors and declines in rod-driven function.[53,54] Both show increased spontaneous activity levels and increased numbers of visually nonresponsive RGCs.[43,55] Although it is easy to explain a loss of visually responsive RGCs, the observation of why spontaneous activity increases remains an active topic of discussion. Some evidence exists that it may be related to reorganization within the retinal circuit and an absence of signaling from the deafferented rod bipolar cells.[56]

Taken together, our results paint a consistent picture. This transgenic swine model never develops rod vision, although cone vision develops normally for the first month after birth. The presence of a cone-rich visual streak in swine means that therapies developed in this model to preserve cones and their function are likely to translate more readily into preserving central vision in humans. These approaches might include gene therapy or the administration of trophic factors, such as cone viability factor.[57] Another consequence of the unique aspects of this RP model is that it may be used to address the question of why cones die when the primary insult is to the rods. For example, do cones die as a result of a bystander effect with a transfer of toxicity from degenerating rods to cone, do they die from the removal of a trophic factor provided by the rods, or is cone death related to other factors, such as the collapse of outer retina structure?

Acknowledgments

We thank Eric V. Vukmanic, Douglas W. Emery, Leslie Sherwood, DVM, and the University of Louisville Veterinary Care Staff for excellent technical assistance.

Supported by National Institutes of Health (NIH) EY018608, EY140701, (MAM); NIH EY-020647 (HJK); NIH HL076138-08 (JPFdC, JWF); Discovery Eye Foundation; Research to Prevent Blindness, New York, New York, United States; Kentucky Research Challenge Trust Fund (HJK); KY Science and Engineering Foundation (HJK); University of Louisville Clinical and Translational Science Grant (HJK); University of Louisville, School of Medicine, Basic Research Grant (PAS); American Optometric Foundation and Beta Sigma Kappa Optometric Honor Society (PAS); and Fight For Sight (PAS).

Disclosure: **J.P. Fernandez de Castro**, None; **P.A. Scott**, None; **J.W. Fransen**, None; **J. Demas**, None; **P.J. DeMarco**, None; **H.J. Kaplan**, None; **M.A. McCall**, None

References

1. Hamasaki DI, Maguire GW. Physiological development of the kitten's retina: an ERG study. *Vision Res*. 1985;25:1537–1543.
2. Jacobson SG, Ikeda H, Ruddock K. Cone-mediated retinal function in cats during development. *Doc Ophthalmol*. 1987; 65:7–14.
3. Gum GG, Gelatt KN, Samuelson DA. Maturation of the retina of the canine neonate as determined by electroretinography and histology. *Am J Vet Res*. 1984;45:1166–1171.
4. Kirk GR, Boyer SF. Maturation of the electroretinogram in the dog. *Exp Neurol*. 1973;38:252–264.
5. el Azazi M, Wachtmeister L. The postnatal development of the oscillatory potentials of the electroretinogram V. Relation to the double peaked a-wave. *Acta Ophthalmol (Copenh)*. 1993; 71:32–38.
6. el Azazi M, Wachtmeister L. The postnatal development of the oscillatory potentials of the electroretinogram. IV. Mesopic characteristics. *Acta Ophthalmol (Copenh)*. 1992;70:194–200.
7. el Azazi M, Wachtmeister L. The postnatal development of the oscillatory potentials of the electroretinogram. III. Scotopic characteristics. *Acta Ophthalmol (Copenh)*. 1991;69:505–510.
8. el-Azazi M, Wachtmeister L. The postnatal development of the oscillatory potentials of the electroretinogram. I. Basic characteristics. *Acta Ophthalmol (Copenh)*. 1990;68:401–409.
9. Weidman TA, Kuwabara T. Development of the rat retina. *Invest Ophthalmol*. 1969;8:60–69.
10. Ben-Shlomo G, Ofri R. Development of inner retinal function, evidenced by the pattern electroretinogram, in the rat. *Exp Eye Res*. 2006;83:417–423.
11. Gorfinkel J, Lachapelle P. Maturation of the photopic b-wave and oscillatory potentials of the electroretinogram in the neonatal rabbit. *Can J Ophthalmol*. 1990;25:138–144.
12. Gorfinkel J, Lachapelle P, Molotchnikoff S. Maturation of the electroretinogram of the neonatal rabbit. *Doc Ophthalmol*. 1988;69:237–245.
13. Gresh J, Goletz PW, Crouch RK, Rohrer B. Structure-function analysis of rods and cones in juvenile, adult, and aged C57bl/6 and Balb/c mice. *Vis Neurosci*. 2003;20:211–220.
14. Spira AW. In utero development and maturation of the retina of a non-primate mammal: a light and electron microscopic study of the guinea pig. *Anat Embryol (Berl)*. 1975;146:279–300.
15. Hendrickson A, Possin D, Vajzovic L, Toth CA. Histological development of the human fovea from midgestation to maturity. *Am J Ophthalmol*. 2012;145:767–778.
16. De Schaepdrijver L, Lauwers H, Simoens P, De Geest JP. Development of the retina in the porcine fetus. A light microscopic study. *Anat Histol Embryol*. 1990;19:222–235.

17. Smelser GK, Ozanics V, Rayborn M, Sagun D. Retinal synaptogenesis in the primate. *Invest Ophthalmol Vis Sci*. 1974;13:340–361.
18. Fulton AB, Hansen RM, Moskowitz A. Development of rod function in term born and former preterm subjects. *Optom Vis Sci*. 2009;86:653–658.
19. Teller DY. First glances: the vision of infants. The Friedenwald lecture. *Invest Ophthalmol Vis Sci*. 1997;38:2183–2203.
20. Sanchez I, Martin R, Ussa F, Fernandez-Bueno I. The parameters of the porcine eyeball. *Graefes Arch Clin Exp Ophthalmol*. 2011;249:475–482.
21. Braekevelt CR. Fine structure of the retinal rods and cones in the domestic pig. *Graefes Arch Clin Exp Ophthalmol*. 1983; 220:273–278.
22. Beauchemin ML. The fine structure of the pig's retina. *Albrecht Von Graefes Arch Klin Exp Ophthalmol*. 1974;190: 27–45.
23. Moren H, Gesslein B, Andreasson S, Malmsjo M. Multifocal electroretinogram for functional evaluation of retinal injury following ischemia-reperfusion in pigs. *Graefes Arch Clin Exp Ophthalmol*. 2010;248:627–634.
24. Montezuma SR, Loewenstein J, Scholz C, Rizzo JF III. Biocompatibility of materials implanted into the subretinal space of Yucatan pigs. *Invest Ophthalmol Vis Sci*. 2006;47: 3514–3522.
25. Chandler MJ, Smith PJ, Samuelson DA, MacKay EO. Photoreceptor density of the domestic pig retina. *Vet Ophthalmol*. 1999;2:179–184.
26. Gerke CG, Hao Y, Wong F. Topography of rods and cones in the retina of the domestic pig. *Hong Kong Med J*. 1995;1:302–308.
27. Beattie JR, Brockbank S, McGarvey JJ, Curry WJ. Raman microscopy of porcine inner retinal layers from the area centralis. *Mol Vis*. 2007;13:1106–1113.
28. Beattie JR, Brockbank S, McGarvey JJ, Curry WJ. Effect of excitation wavelength on the Raman spectroscopy of the porcine photoreceptor layer from the area centralis. *Mol Vis*. 2005;11:825–832.
29. Hendrickson A, Hicks D. Distribution and density of medium- and short-wavelength selective cones in the domestic pig retina. *Exp Eye Res*. 2002;74:435–444.
30. Prather RS, Lorson M, Ross JW, Whyte JJ, Walters E. Genetically engineered pig models for human diseases. *Annual Reviews in Animal Biosciences*. 2013;1:203–219.
31. Bosse B, Zrenner E, Wilke R. Standard ERG equipment can be used to monitor functionality of retinal implants. *Conf Proc IEEE Eng Med Biol Soc*. 2011;2011:1089–1092.
32. Ghosh F, Engelsberg K, English RV, Petters RM. Long-term neuroretinal full-thickness transplants in a large animal model of severe retinitis pigmentosa. *Graefes Arch Clin Exp Ophthalmol*. 2007;245:835–846.
33. Luu CD, Foulds WS, Kaur C. Electrophysiological findings in a porcine model of selective retinal capillary closure. *Invest Ophthalmol Vis Sci*. 2012;53:2218–2225.
34. Ross JW, Fernandez de Castro JP, Zhao J, et al. Generation of an inbred miniature pig model of retinitis pigmentosa. *Invest Ophthalmol Vis Sci*. 2012;53:501–507.
35. Scott PA, Fernandez de Castro JP, Kaplan HJ, McCall MA. A Pro23His mutation alters prenatal rod photoreceptor morphology in a transgenic swine model of retinitis pigmentosa. *Invest Ophthalmol Vis Sci*. 2014;55:2452–2459.
36. Khaliq S, Abid A, Ismail M, et al. Novel association of RP1 gene mutations with autosomal recessive retinitis pigmentosa. *J Med Genet*. 42:436–438.
37. Avila-Fernandez A, Corton M, Nishiguichi KM, et al. Identification of an RP1 prevalent founder mutation and related phenotype in Spanish patients with early-onset autosomal recessive retinitis pigmentosa. *Ophthalmology*. 2012;119: 2616–2621.
38. Singh HP, Jalali S, Narayanan R, Kannabiran C. Genetic analysis of Indian families with autosomal recessive retinitis pigmentosa by homozygosity screening. *Invest Ophthalmol Vis Sci*. 2009;50:4065–4071.
39. Lalonde MR, Chauhan BC, Tremblay F. Retinal ganglion cell activity from the multifocal electroretinogram in pig: optic nerve section, anaesthesia and intravitreal tetrodotoxin. *J Physiol*. 2006;570:325–338.
40. Marmor MF, Fulton AB, Holder GE, et al. ISCEV standard for full-field clinical electroretinography (2008 update). *Doc Ophthalmol*. 2009;118:69–77.
41. Scott PA, Kaplan HJ, Sandell JH. Anatomical evidence of photoreceptor degeneration induced by iodoacetic acid in the porcine eye. *Exp Eye Res*. 2011;93:513–527.
42. Zhou L, Wang W, Liu Y, et al. Differentiation of induced pluripotent stem cells of swine into rod photoreceptors and their integration into the retina. *Stem Cells*. 2011;29:972–980.
43. Goo YS, Ahn KN, Song YJ, et al. Spontaneous oscillatory rhythm in retinal activities of two retinal degeneration (rd1 and rd10) mice. *Korean J Physiol Pharmacol*. 2011;15:415–422.
44. Fulton AB, Hansen RM, Westall CA. Development of ERG responses: the ISCEV rod, maximal and cone responses in normal subjects. *Doc Ophthalmol*. 2003;107:235–241.
45. Westall CA, Panton CM, Levin AV. Time courses for maturation of electroretinogram responses from infancy to adulthood. *Doc Ophthalmol*. 1998;96:355–379.
46. Fulton AB, Hansen RM. The development of scotopic sensitivity. *Invest Ophthalmol Vis Sci*. 2000;41:1588–1596.
47. Fulton AB, Hansen RM. The relationship of retinal sensitivity and rhodopsin in human infants. *Vision Res*. 1987;27:697–704.
48. Fulton AB, Hansen RM, Moskowitz A. Development of rod function in term born and former preterm subjects. *Optom Vis Sci*. 2009;86:E653–E658.
49. Hansen RM, Fulton AB. Development of the cone ERG in infants. *Invest Ophthalmol Vis Sci*. 2005;46:3458–3462.
50. Sancho-Pelluz J, Arango-Gonzalez B, Kustermann S, et al. Photoreceptor cell death mechanisms in inherited retinal degeneration. *Mol Neurobiol*. 2008;38:253–269.
51. Machida S, Kondo M, Jamison JA, et al. P23H rhodopsin transgenic rat: correlation of retinal function with histopathology. *Invest Ophthalmol Vis Sci*. 2000;41:3200–3209.
52. Martinez-Navarrete G, Seiler MJ, Aramant RB, Fernandez-Sanchez L, Pinilla I, Cuenca N. Retinal degeneration in two lines of transgenic S334ter rats. *Exp Eye Res*. 2011;92:227–237.
53. Gibson R, Fletcher EL, Vingrys AJ, Zhu Y, Vessey KA, Kalloniatis M. Functional and neurochemical development in the normal and degenerating mouse retina. *J Comp Neurol*. 2013;521:1251–1267.
54. Martin RE, Ranchon-Cole I, Brush RS, et al. P23H and S334ter opsin mutations: increasing photoreceptor outer segment n-3 fatty acid content does not affect the course of retinal degeneration. *Mol Vis*. 2004;10:199–207.
55. Stasheff SF. Emergence of sustained spontaneous hyperactivity and temporary preservation of OFF responses in ganglion cells of the retinal degeneration (rd1) mouse. *J Neurophysiol*. 2008; 99:1408–1421.
56. Borowska J, Trenholm S, Awatramani GB. An intrinsic neural oscillator in the degenerating mouse retina. *J Neurosci*. 2011; 31:5000–5012.
57. Yang Y, Mohand-Said S, Danan A, et al. Functional cone rescue by RdCVF protein in a dominant model of retinitis pigmentosa. *Mol Ther*. 2009;17:787–795.

Investigative Ophthalmology & Visual Science